ELSEVIER

Solid State Ionics 97 (1997) 437–441

SOLID STATE IONICS

Fabrication of proton conducting thin films of $SrZrO_3$ and $SrCeO_3$ and their fundamental characterization

N. Sata[a,*], H. Matsuta[a], Y. Akiyama[a], Y. Chiba[a], S. Shin[b], M. Ishigame[b]

[a]*RISM, Tohoku University, 2-1-1 Katahira, Aoba-ku, Sendai 980-77, Japan*
[b]*ISSP, University of Tokyo, 3-2-1 Tanashi, Tokyo 188, Japan*

Abstract

Proton conducting thin films of $SrZrO_3$ and $SrCeO_3$ were fabricated by the pulsed laser ablation method using ArF excimer laser. The thin films of $SrCeO_3$ and $SrZrO_3$ were grown in the [100] direction on the $SrTiO_3$(100) substrate and in the [211] direction on the MgO(100) substrate and on the Al_2O_3 substrate. The Raman scattering spectra show that the thin films grown in the low P_{O_2} contain lots of oxygen ion vacancies compared to bulk crystals.

Keywords: Perovskite-type oxides; Pulsed laser ablation; Thin film

Materials: $SrZrO_3$; $SrCeO_3$

1. Introduction

The acceptor-doped perovskite-type oxides are known as high temperature proton conductors, which are promising materials for devices such as fuel cells, hydrogen sensors and so on [1]. It is known that the proton migrates in the interstitial sites around oxygen ions by hopping in crystals of these proton conductor [2–4]. However, the high proton conductivity in the acceptor-doped perovskite-type oxides has not been understood and the proton conduction mechanism is not yet clear. Raman scattering and XAFS studies of single crystals of these proton conductors suggest that the local lattice distortion caused by acceptor doping plays a very important role for the high proton conductivity [5].

The fabrication techniques of perovskite-type oxides thin films are developed for the growth of ferroelectric thin films, such as $SrTiO_3$ or $BaTiO_3$ [6]. The laser ablation technique is known to be suitable for growth of thin films of these ferroelectric oxides or perovskite-type high T_c superconductors. In this study, the pulsed laser ablation technique was used to fabricate the proton conducting thin films. Studies on proton conductors grown on various substrates will give much information to clarify the relation between the lattice distortion and the proton conductivity. In this paper, the fabrication method of these thin films and their characterization are reported.

2. Experiments

The laser ablation system is shown in Fig. 1. An

*Corresponding author. Tel.: +81-22-217-5346; fax: +81-22-217-5344; e-mail: sata@rism.tohoku.ac.jp

PII S0167-2738(97)00026-X

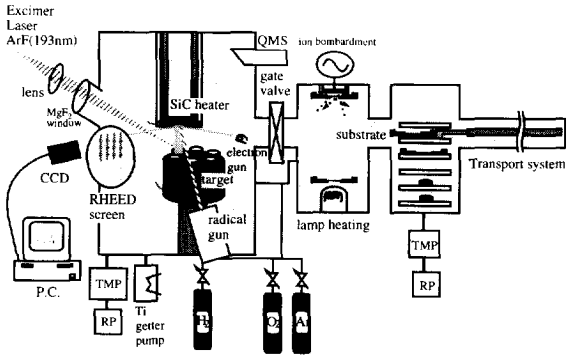

Fig. 1. Laser ablation system used in this study. This system consists of two chambers: One is the ablation chamber and the other is the preparation chamber. The ablation chamber is equipped with a SiC heater (max. 1300°C), an RHEED system, a radical gun and a quadrupole mass spectrometer. The preparation chamber is equipped with an ion bombardment system and a lamp heater (max. 500°C). The MgF_2 window was used.

ArF excimer laser (wavelength 193 nm) was used as the ablation beam. The repetition rate is 1~4 Hz and the laser power is about 400 mJ at the exit mirror of the excimer laser. The ablation targets were sintered ceramics of undoped and acceptor doped $SrZrO_3$ and $SrCeO_3$. Single crystals of $SrTiO_3$, MgO and Al_2O_3 were used for substrates. The substrates and the targets are listed in Table 1 and Table 2, respectively. The films were grown in O_2 atmospheres of about 0.5–1 Pa and the substrates were heated at about 700–900°C. The substrate-target distance was 30~50 mm and target and substrate were rotated during the ablation. The ablation chamber was evacuated to 10^{-7} Pa before the oxygen gas introduction to the chamber. The laser ablation system is equipped with SiC substrate heater (max. 1300°C), radical gun (O radical and H radical), Reflection High Energy Electron Diffraction (RHEED) system and preparation chamber with ion bombardment (RF-sputtering system for substrate cleaning) and lamp heater (max. 500°C).

Total film thickness was about 1000–4000 Å. RHEED image was observed using 20 keV electron beam with diameter about 100 μm. X-ray diffraction (XRD) measurements were performed using the characteristic CuKα line. The Raman scattering study was performed at room temperature using a microscopic-Raman system. The Ar-ion laser (488 nm) was used as a excitation light.

3. Results and discussion

3.1. RHEED

RHEED patterns of $SrCeO_3$ were observed on the Al_2O_3 substrate and those of $SrZrO_3$ and $SrCeO_3$ were observed on the $SrTiO_3$ substrate. However, no RHEED pattern of $SrCeO_3$ was observed on the MgO substrate in this study. It is interesting that the RHEED pattern of $SrCeO_3$ can be observed on the Al_2O_3 and $SrTiO_3$ substrates but not on the MgO, of which crystal parameter matching for $SrCeO_3$ is better than that of Al_2O_3.

The RHEED patterns of the $SrCe_{0.95}Yb_{0.05}O_3$ film deposited on the $SrTiO_3$ (100) substrate are shown in Fig. 2. This pattern changed to (b) about 30 min after

Table 1
Substrates used in this study

Substrate	System	Lattice constant (Å)	Melting point	Band gap
$SrTiO_3$ (100)	Cubic	3.905	1950°C	3.47 eV
MgO (100)	Cubic	4.213	2800°C	7.3 eV
Al_2O_3	Rhomb.	$a=4.758$, $c=12.991$	2030°C	~9 eV

Table 2
Ablation targets for the sputtering of proton conducting thin films

Target	System	Lattice constant (Å)	Dopant	Melting point	Band gap
$SrZrO_3$	Ortho.	$a=8.196$, $b=5.792$, $c=5.814$	Sc, Yb	2700°C	5.96 eV
$SrCeO_3$	Ortho.	$a=8.584$, $b=6.011$, $c=6.155$	Sc, Yb	~1800°C	6 eV

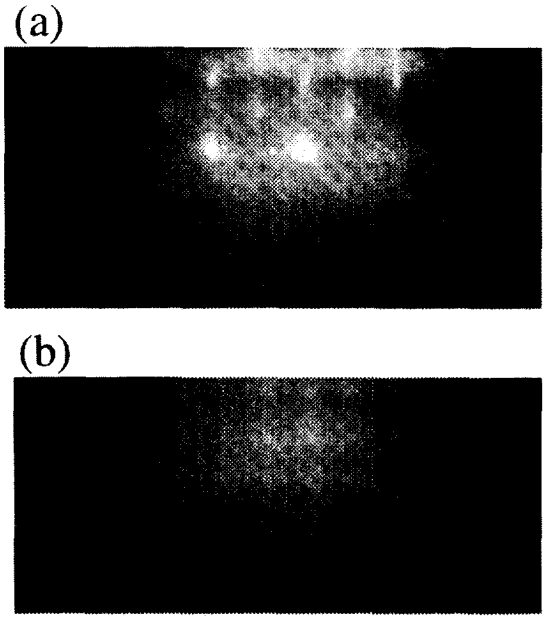

Fig. 2. RHEED patterns of $SrCe_{0.95}Yb_{0.05}O_3$ film deposited on the $SrTiO_3$ (100) substrate at about 850°C. (a) 1 min after the deposition was started. The film thickness is about 6 Å. This pattern was observed for at least 30 min after the deposition was started at the laser repetition rate of 1 Hz. (b) When the deposition was terminated after 166 min. The film thickness is about 1000 Å.

the deposition was started and this pattern was observed when the deposition was terminated. This result suggest that the symmetry of the film surface was changed with film thickness. The pattern (a) was observed even at 750°C of substrate heater temperature, but it faded away soon. When the heater temperature was above 850°C, the RHEED pattern was observed till the end of the deposition.

The RHEED pattern observed on the Al_2O_3 substrate was similar to that of (a) in Fig. 2, but no pattern was observed when the deposition was terminated. The Al_2O_3 substrate surface is fairly flat suggested by the RHEED pattern of Al_2O_3 substrate surface. It is supposed that the $SrCeO_3$ film is well crystallized on the surface of Al_2O_3 up to several layers because of the flatness of the surface, while the crystallinity of the film should be influenced by a strong stress due to large lattice mismatch with the substrate when the film thickness reaches more than several layers.

3.2. X-ray diffraction

The X-ray diffraction spectra of the thin films deposited on the $SrTiO_3$ (100) substrates are shown in Fig. 3. The thin films were deposted at heater temperatures of 730°C–950°C and the substrate temperatures were about 100–150°C lower. The thin films of $SrZrO_3$ and $SrCeO_3$ were grown in the [100] direction of the $SrTiO_3$ substrate as shown in the figure. For $SrCe_{0.95}Yb_{0.05}O_3$ firms, two unknown lines of 2.74 Å and 1.37 Å were observed. These

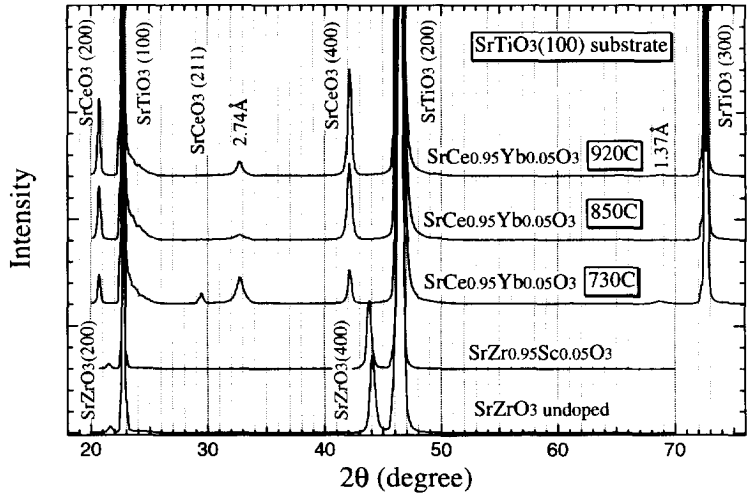

Fig. 3. XRD spectra of $SrZrO_3$ and $SrCe_{0.95}Yb_{0.05}O_3$ deposited on $SrTiO_3$ (100). Values in boxes are substrate heater temperatures. These films were grown in the [100] direction. However, the lines at the d-spacings of 2.74 Å and 1.37 Å correspond to the CeO_2 (200) and (400).

lines correspond to the (200) and (400) lines of CeO_2. It is interesting that the lattice parameter was 0.08 larger in the Sc-doped film than in the undoped film in $SrZrO_3$ films. This difference is often attributed to the large ionic radius of the acceptor ion. However, this lattice parameter enhancement due to the acceptor ion was not observed in $SrCeO_3$ films on the $SrTiO_3$ substrate.

The X-ray diffraction patterns of the thin films deposited on the MgO (100) substrates are shown in Fig. 4. The thin films of $SrZrO_3$ and $SrCeO_3$ were grown in the [211] direction as shown in this figure. The (211) line in undoped $SrCeO_3$ splits into three lines. These lines correspond to (002), (211) and (020) lines of $SrCeO_3$. The line splitting was not observed in the Yb-doped $SrCeO_3$ films.

The crystal structure matching for the $SrZrO_3$ and $SrCeO_3$ should be better on the $SrTiO_3$ substrate, which has the perovskite-type crystal structure similar to $SrZrO_3$ and $SrCeO_3$, than on the MgO substrate, while the lattice constant matching should be better on the MgO substrate. Thin films of $SrCeO_3$–$SrZrO_3$ solid solution were also grown in the [211] direction on the MgO substrate and the lattice parameter of these thin films was enlarged as the $SrCeO_3$ ratio increases.

The samples (a) and (b) of $SrCeO_3$ and $SrCe_{0.95}Yb_{0.05}O_3$ were grown under similar conditions. However, the spectra are different from each other. In samples (b), the CeO_2 peaks were observed and the lattice parameter were slightly enhanced compared with the samples (a). The reason for these differences is not clear.

The [100] direction of $SrZrO_3$ and $SrCeO_3$ corresponds to the [100] direction of cubic perovskite structure such as $SrTiO_3$, while the [211] direction of those corresponds to the [110] direction of $SrTiO_3$. Thin films of $SrZrO_3$ and $SrCeO_3$ grow in the same direction as $SrTiO_3$ on the $SrTiO_3$ substrate, while they grow in the [110] direction on the MgO and the Al_2O_3 substrates. The X-ray diffraction results suggest that the growth direction of the thin films depends on the arrangement of atoms of substrate but not on its lattice parameter.

3.3. Raman scattering

Raman scattering spectra of proton conducting thin films and single crystals are shown in Fig. 5. The Raman spectra of the thin films and the single crystals resemble each other. However, in the thin film of $SrCe_{0.98}Yb_{0.02}O_3$, the high frequency modes above 500 cm^{-1} and the Raman band at about 350 cm^{-1} shift to higher frequency compared to those in single crystals. The Raman bands around 300–375 cm^{-1} correspond to the CeO_6 stretching modes on the analogy of those in $BaCeO_3$ [7]. It is suggested that the Raman structure around 500–700 cm^{-1} is

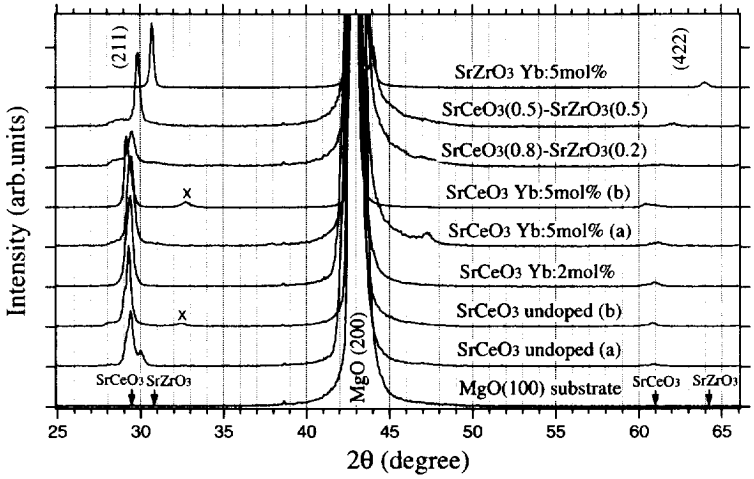

Fig. 4. XRD spectra of $SrZrO_3$, $SrCeO_3$ and their solid solutions ($SrZrO_3$–$SrCeO_3$) deposited on MgO (100). Arrows at the bottom of this graph indicate the (211) and (422) of $SrZrO_3$ and $SrCeO_3$. The impurity line marked with '×' is the CeO_2 (200) line.

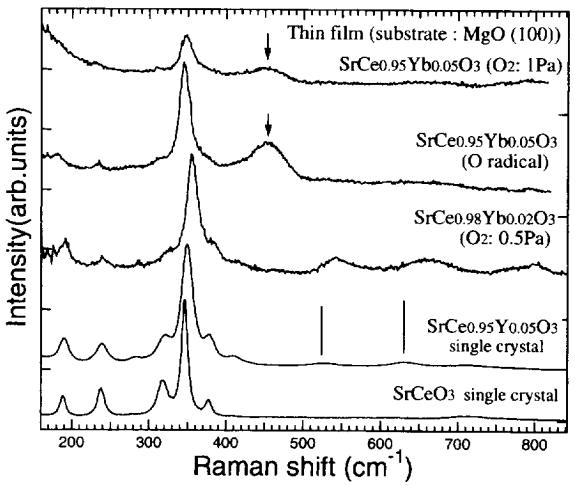

Fig. 5. Raman scattering spectra of $SrCeO_3$ thin film and single crystal. Arrows at 455 cm^{-1} indicate the Raman band of CeO_2.

connected with distortion due to oxygen ion vacancies [7]. It is recognized that the oxygen vacancy concentration in this thin film is larger than in the bulk single crystals.

On the other hand for $SrCe_{0.95}Yb_{0.05}O_3$ thin films which were grown under high oxygen gas pressure or under O-radical irradiation, those frequency shifts were not observed and the intensity of the high frequency modes above 500 cm^{-1} is not so different from that in the single crystal of $SrCe_{0.95}Y_{0.05}O_3$. The impurity structure at 455 cm^{-1} corresponds to the Raman band of CeO_2, which is consistent with the result of X-ray diffraction.

4. Summary

Proton conducting thin films of $SrZrO_3$, $SrCeO_3$ and $SrCeO_3$–$SrZrO_3$ solid solution were fabricated by the pulsed laser ablation method. The films were grown in a certain direction depending on the substrates. The synthesized thin films contain high concentrations of oxygen ion vacancies when deposited in 0.5 Pa O_2, decreasing when O-radicals were irradiated or in higher oxygen gas pressure, as indicated by the Raman scattering study. The X-ray and Raman experiments showed that the $SrCeO_3$ thin films are contaminated by CeO_2, which is a serious problem for fabrication of proton conducting thin films of good quality.

Acknowledgments

This work is supported by the Grant-in-aid for Scientific research on Priority Areas (No. 260) from The Ministry of Education, Science, Sports and Culture, Japan.

References

[1] H. Iwahara, T. Esaka, H. Uchida, N. Maeda, Solid State Ionics 3/4 (1981) 359.
[2] H.H. Huang, M. Ishigame, S. Shin, Solid State Ionics 47 (1991) 251.
[3] S. Shin, H.H. Huang, M. Ishigame, H. Iwahara, Solid State Ionics 40/41 (1990) 910.
[4] N. Sata, K. Hiramoto, M. Ishigame, S. Hosoya, N. Niimura, S. Shin, Phys. Rev. B 54 (1996) 15795.
[5] N. Sata, S. Shin and M. Ishigame, unpublished.
[6] M. Yoshimoto, H. Ohkubo, N. Kanda, H. Koinuma, Jpn. J. Appl. Phys. 31 (1992) 3664.
[7] T. Scherban, R. Villeneuve, L. Abello, G. Lucazeau, Solid State Ionics 61 (1993) 93.